Next-to-leading order QCD corrections to $Z \to \eta_Q + Q + \bar{Q}$

Xu-Chang Zheng,[1,*] Xing-Gang Wu,[1,†] Xi-Jie Zhan,[1,‡] Hua Zhou,[1,2,§] and Hong-Tai Li[1,‖]

[1]*Department of Physics, Chongqing Key Laboratory for Strongly Coupled Physics, Chongqing University, Chongqing 401331, People's Republic of China*

[2]*Department of Physics, Norwegian University of Science and Technology, Høgskoleringen 5, N-7491 Trondheim, Norway*

(Received 10 May 2022; revised 4 September 2022; accepted 11 October 2022; published 4 November 2022)

It has been found that at a high luminosity e^+e^- collider, sizable $\eta_c + c\bar{c}X$, and $\eta_b + b\bar{b}X$ events can be produced when it works around the Z peak. In this paper, we calculate the decay widths of $Z \to \eta_c + c + \bar{c} + X$ and $Z \to \eta_b + b + \bar{b} + X$ up to next-to-leading order (NLO) accuracy. We find that the NLO corrections are significant in these two processes. After including the NLO corrections, the decay widths of $Z \to \eta_c + c + \bar{c} + X$ and $Z \to \eta_b + b + \bar{b} + X$ are enhanced by about 34% and 28% for the case of $\mu_R = 2m_Q$, and are enhanced by about 112% and 83% for the case of $\mu_R = m_Z$, respectively. The differential decay widths $d\Gamma/dz$, $d\Gamma/dm_{12}$, and $d\Gamma/dm_{23}$ for these two decay processes are also analyzed.

DOI: 10.1103/PhysRevD.106.094008

I. INTRODUCTION

Heavy quarkonium production presents an ideal laboratory for the study of the interplay between the perturbative and nonperturbative effects of QCD; it has been a focus of theoretical and experimental interest since the discovery of J/ψ in 1974. In order to describe the quarkonium production, the color-evaporation model (CEM) [1,2], the color-singlet model (CSM) [3–5], and the nonrelativistic QCD (NRQCD) effective theory [6] have been proposed. Among them, the NRQCD effective theory provides a systematic way of separating the short-distance and long-distance effects in the quarkonium production, and has achieved great success in describing the experimental data of the quarkonium production, especially for the unpolarized cross section of the J/ψ hadroproduction [7–10]. However, there are still challenges to NRQCD. For instance, the hadroproduction cross section of η_c measured by the LHCb experiments [11] can be well described by the color-singlet contribution, i.e., the color-octet contribution should be very small [12]. This seems inconsistent with the heavy-quark spin symmetry (HQSS) relation between the long-distance matrix elements (LDMEs) of η_c and J/ψ.[1] It is important to study more processes involving the charmonium for testing the NRQCD factorization.

It has been found that the heavy quarkonium production through Z boson decays can provide a good platform for studying the production mechanism of quarkonia, which has attracted great attention [17–39]. A large number of Z boson events can be accumulated at the LHC or a future high-luminosity e^+e^- collider running around the Z pole. At the LHC, there are about 10^9 Z bosons to be produced per year [29]. It is well known that several proposed high-luminosity e^+e^- colliders, such as the ILC [40], FCC-ee [41], CEPC [42], and Super Z Factory [43], are planned to run at the Z pole for a period of time. When the e^+e^- collider runs at the Z pole and with a luminosity of 10^{34-36} cm^{-2} s^{-1}, there are about 10^{9-11} Z bosons to be produced per year [44]. These colliders will open new opportunities for studying the quarkonium production through Z boson decays.

Most studies on the heavy quarkonium production through the Z boson decays focus on the spin-triplet J/ψ and Υ production, while few studies are for the spin-singlet η_Q ($Q = b$ or c) production. In our recent work [38], we studied the inclusive production of the η_Q via the Z boson decays up to order $\alpha\alpha_s^2$ within the framework of NRQCD,

*zhengxc@cqu.edu.cn
†wuxg@cqu.edu.cn
‡zhanxj@cqu.edu.cn
§zhouhua@cqu.edu.cn
‖liht@cqu.edu.cn

[1]References [13,14] pointed out that the hadroproduction data of J/ψ and η_c can be simultaneously described by one set of LDMEs. However, theoretical predictions based on this set of LDMEs fail to describe the J/ψ production data from e^+e^- annihilation at the B-factory [15,16].

in which the leading color-singlet ($^1S_0^{[1]}$) and color-octet ($^1S_0^{[8]}$, $^3S_1^{[8]}$, and $^1P_1^{[8]}$) Fock states are considered. The study found that there are many interesting features in these production processes. An important channel contributing to the inclusive production $Z \to \eta_Q + X$ is $Z \to \eta_Q + Q + \bar{Q}$. Experimentally, its decay width can be measured separately through the heavy-flavor tagging technology. Therefore, it is helpful to do a precise theoretical study on this channel. In this paper, we devote ourselves to studying the decay $Z \to \eta_Q + Q + \bar{Q} + X$, which starts at order $\alpha\alpha_s^2$, up to NLO QCD accuracy. We will use the CSM, which is the leading-order (LO) contribution (in v_Q, where v_Q is the velocity of the heavy quark or the heavy antiquark in the quarkonium rest frame, $v_c^2 \approx 30\%$ for the η_c and $v_b^2 \approx 10\%$ for the η_b [45]) of NRQCD,[2] to calculate the decay width of $Z \to \eta_Q + Q + \bar{Q} + X$.

The NLO QCD corrections to $Z \to \eta_Q + gg$ have recently been finished through the CSM [39]. The authors there found that the NLO corrections are significant due to the fragmentation diagrams appearing at the NLO level.[3] Reference [39] and the present paper give a complete study on the η_Q production through Z boson decays up to NLO QCD accuracy under the CSM.

The remaining parts of the paper are organized as follows. In Sec. II, we briefly present useful formulas for the process $Z \to \eta_Q + Q + \bar{Q} + X$ at the LO accuracy. In Sec. III, we present the formulas for calculating the NLO QCD corrections to the process $Z \to \eta_Q + Q + \bar{Q} + X$. In Sec. IV, numerical results and discussions are presented. Section V is reserved as a summary.

II. LO DECAY WIDTH

Under the NRQCD factorization, the decay width for $Z \to \eta_Q + Q + \bar{Q} + X$ can be written as

$$d\Gamma_{Z\to\eta_Q+Q+\bar{Q}+X} = \sum_n d\tilde{\Gamma}_{Z\to(Q\bar{Q})[n]+Q+\bar{Q}+X}\langle\mathcal{O}^{\eta_Q}(n)\rangle, \quad (1)$$

where $d\tilde{\Gamma}$ are short-distance coefficients (SDCs) and $\langle\mathcal{O}^{\eta_c}(n)\rangle$ are LDMEs. The sum extends over all of the intermediate color-singlet and color-octet states $^{2S+1}L_J^{[1,8]}$. In the lowest-order nonrelativistic approximation (i.e., the CSM), only the color-singlet contribution with $n = {}^1S_0^{[1]}$ needs to be considered.

In the practical calculation, we first calculate the decay width for a free on-shell $(Q\bar{Q})$ pair with quantum number $^1S_0^{[1]}$, i.e., $d\Gamma_{Z\to(Q\bar{Q})[^1S_0^{[1]}]+Q+\bar{Q}+X}$. Then the decay width for the η_Q meson can be obtained from $d\Gamma_{Z\to(Q\bar{Q})[^1S_0^{[1]}]+Q+\bar{Q}+X}$ through replacing $\langle\mathcal{O}^{(Q\bar{Q})[^1S_0^{[1]}]}(^1S_0^{[1]})\rangle$ by $\langle\mathcal{O}^{\eta_Q}(^1S_0^{[1]})\rangle$.

At the LO level, there are four Feynman diagrams for the decay process $Z \to (Q\bar{Q})[^1S_0^{[1]}] + Q + \bar{Q}$, which are shown in Fig. 1. Corresponding to the four Feynman diagrams, the LO amplitude for this process can be written as $M_{\rm LO} = M_1 + M_2 + M_3 + M_4$, where

$$\begin{aligned} iM_1 = &-\frac{ig}{2\cos\theta_W}\frac{-i}{(p_1/2+p_2)^2+i\epsilon}\bar{u}(p_2)(ig_s\gamma^\mu T^a) \\ &\cdot\Pi_1\Lambda_1(ig_s\gamma_\mu T^a)\frac{i}{\not{p}_1+\not{p}_2-m_Q+i\epsilon}\epsilon_\nu(p_0)\gamma^\nu \\ &\cdot(V_Q - A_Q\gamma_5)v(p_3), \end{aligned} \quad (2)$$

$$\begin{aligned} iM_2 = &-\frac{ig}{2\cos\theta_W}\frac{-i}{(p_1/2+p_2)^2+i\epsilon}\bar{u}(p_2)(ig_s\gamma^\mu T^a)\Pi_1 \\ &\cdot\Lambda_1\epsilon_\nu(p_0)\gamma^\nu(V_Q - A_Q\gamma_5)\frac{i}{-\not{p}_0+\not{p}_1/2-m_Q+i\epsilon} \\ &\cdot(ig_s\gamma_\mu T^a)v(p_3), \end{aligned} \quad (3)$$

$$\begin{aligned} iM_3 = &-\frac{ig}{2\cos\theta_W}\frac{-i}{(p_1/2+p_3)^2+i\epsilon}\bar{u}(p_2)\epsilon_\nu(p_0)\gamma^\nu \\ &\cdot(V_Q - A_Q\gamma_5)\frac{i}{-\not{p}_1-\not{p}_3-m_Q+i\epsilon}(ig_s\gamma_\mu T^a) \\ &\cdot\Pi_1\Lambda_1(ig_s\gamma^\mu T^a)v(p_3), \end{aligned} \quad (4)$$

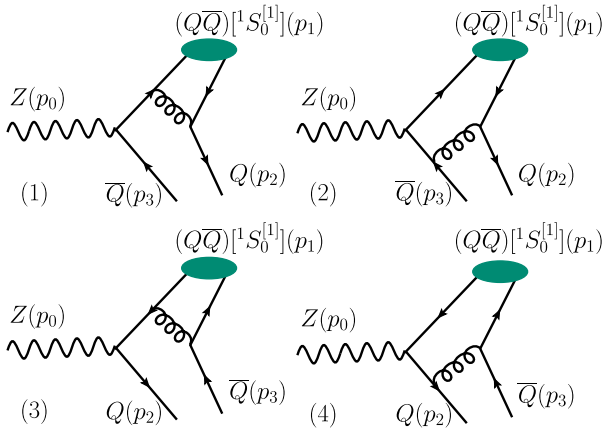

FIG. 1. The LO Feynman diagrams for $Z \to (Q\bar{Q})[^1S_0^{[1]}] + Q + \bar{Q}$.

[2]The next-order relativistic correction to the color-singlet contribution is suppressed by order v_Q^2, while the color-octet contribution is suppressed by order v_Q^4. It is noted that the short-distance factor of the color-octet contribution may be enhanced compared to that of the color-singlet contribution. In this work, we assume the color-octet contribution is very small, and focus on the color-singlet contribution.

[3]The large fragmentation contribution in the NLO corrections of $Z \to \eta_Q + gg$ can be calculated through the fragmentation-function approach, where the large logarithms of m_Z/m_Q in higher-order corrections can be resummed through the Dokshitzer-Gribov-Lipatov-Altarelli-Parisi (DGLAP) evolution of the fragmentation functions [46].

$$iM_4 = -\frac{ig}{2\cos\theta_W}\frac{-i}{(p_1/2+p_3)^2+i\epsilon}\bar{u}(p_2)(ig_s\gamma_\mu T^a)\cdot\frac{i}{\not p_0-\not p_1/2-m_Q+i\epsilon}\epsilon_\nu(p_0)\gamma^\nu(V_Q-A_Q\gamma_5)\cdot\Pi_1\Lambda_1(ig_s\gamma^\mu T^a)v(p_3). \quad (5)$$

Here, V_Q and A_Q are vector and axial electroweak couplings, respectively. More explicitly, $V_c=\frac{1}{2}-\frac{4}{3}\sin^2\theta_W$, $A_c=\frac{1}{2}$, $V_b=-\frac{1}{2}+\frac{2}{3}\sin^2\theta_W$, and $A_b=-\frac{1}{2}$. Π_1 is the projector for S-wave spin-singlet state

$$\Pi_1=\frac{1}{(2m_Q)^{3/2}}(\not p_1/2-m_Q)\gamma_5(\not p_1/2+m_Q), \quad (6)$$

and Λ_1 is the color projector for color-singlet state

$$\Lambda_1=\frac{\mathbf{1}}{\sqrt{3}}, \quad (7)$$

where 1 is the unit matrix of the $SU(3)_c$ group.

With these amplitudes, the LO decay width for the $(Q\bar{Q})[^1S_0^{[1]}]$ pair can be calculated through

$$d\Gamma_{\rm LO}^{(Q\bar{Q})[^1S_0^{[1]}]}=\frac{1}{3}\frac{1}{2m_Z}\sum|M_{\rm LO}|^2d\Phi_3, \quad (8)$$

where $\sum$ denotes the sum over the spin and color states of initial and final particles. $d\Phi_3$ is the differential phase space for the three-body final state, and

$$d\Phi_3=(2\pi)^d\delta^d\left(p_0-\sum_{f=1}^{3}p_f\right)\prod_{f=1}^{3}\frac{d^{d-1}\mathbf{p}_f}{(2\pi)^{d-1}2E_f}, \quad (9)$$

where d is the number of the space-time dimensions. With these formulas, the LO decay width for $Z\to(Q\bar{Q})[^1S_0^{[1]}]+Q+\bar{Q}$ can be calculated directly.

III. NLO CORRECTIONS

At the NLO level, the virtual and real corrections need to be calculated. There are ultraviolet (UV) and infrared (IR) divergences in virtual correction, and IR divergence in real correction. The conventional dimensional regularization with $d=4-2\epsilon$ is employed to regularize both UV and IR divergences throughout this paper. In dimensional regularization, the γ_5 problem is notorious, and we adopt a practical prescription proposed in Ref. [47]. In the following subsections, we explain our main steps in calculating the virtual and real corrections.

A. Virtual NLO correction

The virtual correction at the NLO level comes from the interference of the one-loop Feynman diagrams and the LO Feynman diagrams. Four typical one-loop Feynman diagrams are shown in Fig. 2. It is noted that, compared to the J/ψ case [28], there are new type Feynman diagrams, in which the $(Q\bar{Q})[^1S_0^{[1]}]$ pair is produced from two virtual gluons, need to be calculated in the η_Q case. These new type Feynman diagrams do not contribute to the J/ψ case. One of the new type diagrams is shown by the fourth diagram in Fig. 2.

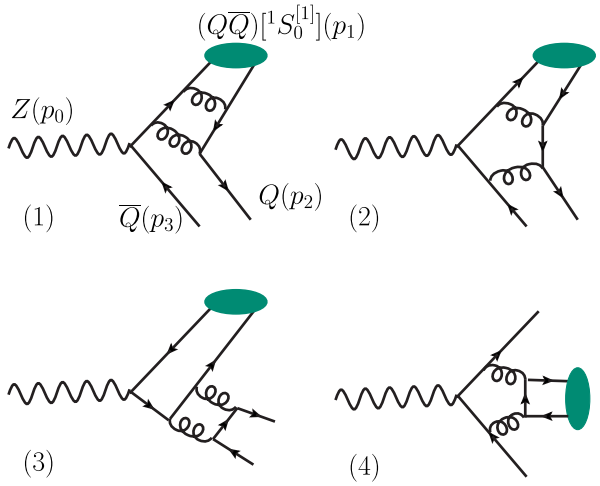

FIG. 2. Four typical one-loop Feynman diagrams for $Z\to(Q\bar{Q})[^1S_0^{[1]}]+Q+\bar{Q}$.

The virtual correction to the decay width of the process $Z\to(Q\bar{Q})[^1S_0^{[1]}]+Q+\bar{Q}$ can be calculated through

$$d\Gamma_{\rm Virtual}^{(Q\bar{Q})[^1S_0^{[1]}]}=\frac{1}{3}\frac{1}{2m_Z}\sum 2{\rm Re}(M_{\rm LO}^*M_{\rm Virtual})d\Phi_3, \quad (10)$$

where $M_{\rm Virtual}$ is the amplitude for the virtual correction, and $d\Phi_3$ is the differential three-body phase space, which has been presented in Eq. (9).

In order to take the lowest-order nonrelativistic approximation, we need to expand the amplitude in q [the relative momentum between the quark and antiquark in the $(Q\bar{Q})[^1S_0^{[1]}]$ pair]. In the actual calculation, we expand the amplitude in q (it is equivalent to taking $q=0$ here) before performing the loop integration. In the language of method of region [48], this amounts to directly calculating the contributions from the hard region. The Coulomb divergence, which is power IR divergence, will vanish in the calculation under dimensional regularization.

There are UV and IR divergences in the loop integrals. The IR divergences from the virtual correction will be canceled by the IR divergences from the real correction. The UV divergences need to be removed through renormalization. The renormalization scheme is taken as follows: For the renormalization of the heavy quark field, the heavy quark mass and the gluon field, the on-mass-shell (OS) scheme is adopted, while for the renormalization of the

strong coupling constant, the modified minimal subtraction ($\overline{\rm MS}$) scheme is adopted. With this renormalization scheme, the quantities $\delta Z_i \equiv Z_i - 1$ can be derived [49]

$$\begin{aligned}
\delta Z_{2,Q}^{\rm OS} &= -C_F \frac{\alpha_s}{4\pi}\left[\frac{1}{\epsilon_{\rm UV}} + \frac{2}{\epsilon_{\rm IR}} - 3\gamma_E + 3\ln\frac{4\pi\mu_R^2}{m_Q^2} + 4\right],\\
\delta Z_{m,Q}^{\rm OS} &= -3C_F \frac{\alpha_s}{4\pi}\left[\frac{1}{\epsilon_{\rm UV}} - \gamma_E + \ln\frac{4\pi\mu_R^2}{m_Q^2} + \frac{4}{3}\right],\\
\delta Z_3^{\rm OS} &= \frac{\alpha_s}{4\pi}\left[(\beta_0' - 2C_A)\left(\frac{1}{\epsilon_{\rm UV}} - \frac{1}{\epsilon_{\rm IR}}\right)\right.\\
&\quad \left. -\frac{4}{3}T_F\sum_Q\left(\frac{1}{\epsilon_{\rm UV}} - \gamma_E + \ln\frac{4\pi\mu_R^2}{m_c^2}\right)\right],\\
\delta Z_g^{\overline{\rm MS}} &= -\frac{\beta_0}{2}\frac{\alpha_s}{4\pi}\left[\frac{1}{\epsilon_{\rm UV}} - \gamma_E + \ln(4\pi)\right],
\end{aligned} \tag{11}$$

where μ_R is the renormalization scale, γ_E is the Euler constant. $\beta_0 = 11C_A/3 - 4T_F n_f/3$ is the one-loop coefficient of the QCD β function, in which n_f is the number of active quark flavors. $\beta_0' = 11C_A/3 - 4T_F n_{lf}/3$ and $n_{lf} = 3$ is the number of light-quark flavors. When $\mu_R \in [m_c, m_b)$, we consider the charm-quark loop in the gluon self-energy but neglect the bottom-quark and top-quark loops in the gluon self-energy, i.e., $n_f = n_{lf} + 1 = 4$; when $\mu_R \in [m_b, m_t)$, we consider the charm-quark and bottom-quark loops in the gluon self-energy but neglect the top-quark loop in the gluon self-energy, i.e., $n_f = n_{lf} + 2 = 5$. For $SU(3)_c$ group, $C_A = 3$, $C_F = 4/3$ and $T_F = 1/2$.

In the calculations, the package FeynArts [50] is employed to generate Feynman diagrams and amplitudes, the package FeynCalc [51,52] is employed to carry out the color and Dirac traces, the packages \$Apart [53] and FIRE [54] are employed to conduct partial fraction and integration-by-parts (IBP) reduction. After the IBP reduction, all one-loop integrals are reduced into master integrals, and the master integrals are calculated by the package LoopTools [55] numerically. The final phase-space integrations are calculated with the help of the package Vegas [56].

B. Real NLO correction

The real correction to the process $Z \to (Q\bar{Q})[^1S_0^{[1]}] + Q + \bar{Q}$ comes from the process $Z(p_0) \to (Q\bar{Q})[^1S_0^{[1]}](p_1) + Q(p_2) + \bar{Q}(p_3) + g(p_4)$. Four typical Feynman diagrams are shown in Fig. 3. Compared to the J/ψ case, we need to deal with new type Feynman diagrams, in which the $(Q\bar{Q})[^1S_0^{[1]}]$ pair is produced from the gluon fragmentation, such as in the fourth diagram of Fig. 3.

Using these Feynman diagrams, the amplitude ($M_{\rm Real}$) for the real correction can be written down directly. Then the differential decay width for the real correction can be calculated through

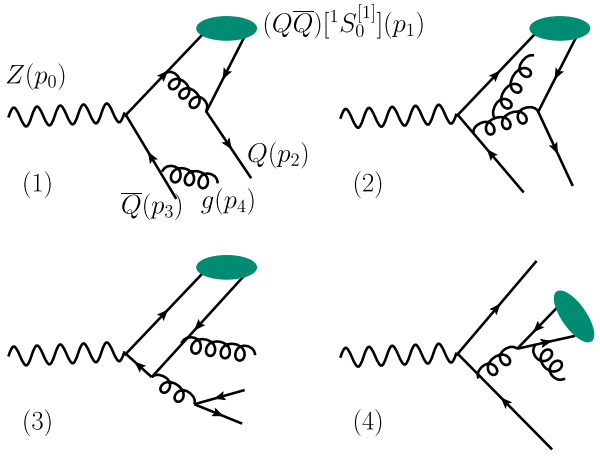

FIG. 3. Four typical real-correction Feynman diagrams for the decay process, $Z \to (Q\bar{Q})[^1S_0^{[1]}] + Q + \bar{Q}$.

$$d\Gamma_{\rm Real}^{(Q\bar{Q})[^1S_0^{[1]}]} = \frac{1}{3}\frac{1}{2m_Z}\sum |M_{\rm Real}|^2 d\Phi_4, \tag{12}$$

where $d\Phi_4$ is the differential four-body phase space,

$$d\Phi_4 = (2\pi)^d \delta^d\left(p_0 - \sum_{f=1}^4 p_f\right)\prod_{f=1}^4 \frac{d^{d-1}\mathbf{p}_f}{(2\pi)^{d-1}2E_f}. \tag{13}$$

There are IR divergences in the real correction, which come from the phase-space integration over the region where the momentum of the final gluon is close to zero. We employ the two-cutoff phase-space slicing method [57] to isolate the IR divergences in the real correction. Due to the fact that there is no collinear divergence in the present process, we only need to introduce one cutoff parameter δ_s. Then the phase space for the real correction is divided into two regions: The soft region with $E_4 \le m_Z\delta_s/2$ and the hard region with $E_4 > m_Z\delta_s/2$. Here, we define the gluon energy E_4 in the rest frame of the initial Z boson. More explicitly, the real correction can be divided into two parts

$$d\Gamma_{\rm Real}^{(Q\bar{Q})[^1S_0^{[1]}]} = d\Gamma_{\rm S}^{(Q\bar{Q})[^1S_0^{[1]}]} + d\Gamma_{\rm H}^{(Q\bar{Q})[^1S_0^{[1]}]}, \tag{14}$$

where

$$d\Gamma_{\rm S}^{(Q\bar{Q})[^1S_0^{[1]}]} = \frac{1}{3}\frac{1}{2m_Z}\sum |M_{\rm Real}|^2 d\Phi_4|_{E_4 \le m_Z\delta_s/2}, \tag{15}$$

and

$$d\Gamma_{\rm H}^{(Q\bar{Q})[^1S_0^{[1]}]} = \frac{1}{3}\frac{1}{2m_Z}\sum |M_{\rm Real}|^2 d\Phi_4|_{E_4 > m_Z\delta_s/2}. \tag{16}$$

Applying the eikonal approximation to the amplitude in the soft region [57,58], we obtain

$$\sum |M_{\rm Real}|^2|_{E_4\le m_Z\delta_s/2} = 4\pi\alpha_s C_F\mu_R^{2\epsilon}\left[-\frac{p_2^2}{(p_2\cdot p_4)^2}+\frac{2p_2\cdot p_3}{(p_2\cdot p_4)(p_3\cdot p_4)} -\frac{p_3^2}{(p_3\cdot p_4)^2}\right]\sum|M_{\rm LO}|^2. \quad (17)$$

Up to $\mathcal{O}(\delta_s)$ corrections, the differential phase space for the soft region can be factorized as [57]

$$d\Phi_4|_{E_4\le m_Z\delta_s/2} = d\Phi_3\left.\frac{d^{d-1}\mathbf{p}_4}{(2\pi)^{d-1}2E_4}\right|_{E_4\le m_Z\delta_s/2}, \quad (18)$$

where $d\Phi_3$ denotes the differential three-body phase space without emitting a gluon, whose expression has been shown in Eq. (9).

Inserting Eqs. (17) and (18) into Eq. (15), and carrying out the integration over p_4 [59,60], we obtain

$$d\Gamma_{\rm S}^{(Q\bar{Q})[^1S_0^{[1]}]} = d\Gamma_{\rm LO}^{(Q\bar{Q})[^1S_0^{[1]}]}\left[\frac{C_F\alpha_s\Gamma(1+\epsilon)}{\pi}\left(\frac{4\pi\mu_R^2}{m_Z^2}\right)^{\epsilon}\right]\left\{\left(\frac{1}{\epsilon}-\ln\delta_s^2\right)\left(1-\frac{\kappa p_2\cdot p_3}{(\kappa^2-1)m_Q^2}\ln\kappa^2\right)+\frac{1}{2\beta_2}\ln\left(\frac{1+\beta_2}{1-\beta_2}\right) +\frac{1}{2\beta_3}\ln\left(\frac{1+\beta_3}{1-\beta_3}\right)+\frac{2\kappa p_2\cdot p_3}{(\kappa^2-1)m_Q^2}\left[\frac{1}{4}\ln^2\frac{u^0-|\mathbf{u}|}{u^0+|\mathbf{u}|}+{\rm Li}_2\left(1-\frac{u^0+|\mathbf{u}|}{v}\right)+{\rm Li}_2\left(1-\frac{u^0-|\mathbf{u}|}{v}\right)\right]\Big|_{u=p_3}^{u=\kappa p_2}\right\}, \quad (19)$$

where

$$\beta_2=\sqrt{1-m_Q^2/E_2^2},\quad \beta_3=\sqrt{1-m_Q^2/E_3^2},\quad v=\frac{(\kappa^2-1)m_Q^2}{2(\kappa E_2-E_3)},\quad \kappa=\frac{p_2\cdot p_3+\sqrt{(p_2\cdot p_3)^2-m_Q^4}}{m_Q^2},$$

where E_2 and E_3 are also defined in the rest frame of the initial Z boson.

Due to the constraint $E_4 > m_Z\delta_s/2$ for the hard region, the contribution from the hard region is finite, then $\Gamma_{\rm H}^{(Q\bar{Q})[^1S_0^{[1]}]}$ can be numerically calculated in four dimensions. The real correction can be obtained by summing the contributions from the hard and soft regions easily. Both the contributions from the soft and hard regions are separately dependent on the cutoff parameter δ_s, while the sum of these two contributions should be independent to the choice of δ_s (δ_s should be small enough.). Verifying this δ_s independence is an important test of the correctness of the calculation. We have checked the δ_s independence, and have found that the results are independent of δ_s within the error of the numerical integration when δ_s varies from 10^{-5} to 10^{-7}.

The net NLO corrections can be obtained through summing the virtual and real corrections. After summing the virtual and real corrections, the UV and IR divergences are exactly canceled, and the finite results are obtained. The decay width $d\Gamma_{Z\to\eta_Q+Q\bar{Q}X}$ can be obtained from $d\Gamma_{Z\to(Q\bar{Q})[^1S_0^{[1]}]+Q\bar{Q}X}$ by multiplying a factor $\langle\mathcal{O}^{\eta_Q}(^1S_0^{[1]})\rangle/\langle\mathcal{O}^{(Q\bar{Q})[^1S_0^{[1]}]}(^1S_0^{[1]})\rangle \approx |R_{\eta_Q}(0)|^2/(4\pi)$, where $R_{\eta_Q}(0)$ is η_Q radial wave function at the origin, which can be calculated by using the potential model [61].

IV. NUMERICAL RESULTS AND DISCUSSIONS

The input parameters for the numerical calculation are taken as follows [62]:

$$m_c=1.67\pm0.07\,{\rm GeV},\quad m_b=4.78\pm0.06\,{\rm GeV},$$
$$m_Z=91.1876\,{\rm GeV},\quad \sin^2\theta_W=0.231,\quad \alpha=1/128, \quad (20)$$

where m_c and m_b are the pole masses, α is the electromagnetic coupling constant at m_Z. For the running strong coupling constant, we use the two-loop formula

$$\alpha_s(\mu_R)=\frac{4\pi}{\beta_0\ln(\mu_R^2/\Lambda_{\rm QCD}^2)}\left[1-\frac{\beta_1\ln\ln(\mu_R^2/\Lambda_{\rm QCD}^2)}{\beta_0^2\ln(\mu_R^2/\Lambda_{\rm QCD}^2)}\right], \quad (21)$$

where $\beta_1=34C_A^2/3-4T_FC_Fn_f-20T_FC_An_f/3$ is the two-loop coefficient of the QCD β function. According to $\alpha_s(m_Z)=0.118$ [62], we obtain $\Lambda_{\rm QCD}^{n_f=5}=0.226$ GeV and $\Lambda_{\rm QCD}^{n_f=4}=0.328$ GeV. With the values for $\Lambda_{\rm QCD}$, the strong coupling constant at any scale can be directly calculated through Eq. (21). For the radial wave functions at the origin, we adopt the values from the potential-model calculation [61], i.e.,

$$|R_{\eta_c}(0)|^2=0.810\,{\rm GeV}^3,\quad |R_{\eta_b}(0)|^2=6.477\,{\rm GeV}^3. \quad (22)$$

A. Integrated decay widths

In this subsection, we give the integrated decay widths for the decay channel $Z\to\eta_Q+Q+\bar{Q}+X$ up to the NLO level.

In order to have a glance on the size of the NLO corrections, we first present the decay widths when the

TABLE I. The decay width (in unit keV) of $Z\to\eta_c+c+\bar{c}+X$ up to the NLO level under two different choices of μ_R, where the input charm quark mass is taken as the central value (i.e. $m_c=1.67$ GeV) and the K factor is defined as $K=\Gamma_{\rm NLO}/\Gamma_{\rm LO}$.

μ_R	$\alpha_s(\mu_R)$	$\Gamma_{\rm LO}$	$\Gamma_{\rm NLO}$	K
$2m_c$	0.245	62.7	84.3	1.34
m_Z	0.118	14.5	30.8	2.12

TABLE II. The decay width (in unit keV) of $Z\to\eta_b+b+\bar{b}+X$ up to the NLO level under two different choices of μ_R, where the input bottom quark mass is taken as the central value (i.e. $m_b=4.78$ GeV) and the K factor is defined as $K=\Gamma_{\rm NLO}/\Gamma_{\rm LO}$.

μ_R	$\alpha_s(\mu_R)$	$\Gamma_{\rm LO}$	$\Gamma_{\rm NLO}$	K
$2m_b$	0.180	10.8	13.8	1.28
m_Z	0.118	4.65	8.49	1.83

input quark masses are taken as their central values (i.e., $m_c=1.67$ GeV and $m_b=4.78$ GeV), an analysis of the uncertainties of these decay widths will be presented later. The decay widths of $Z\to\eta_Q+Q+\bar{Q}+X$ up to the NLO level are given in Tables I and II, where $\Gamma_{\rm NLO}$ denotes the sum of the LO contribution and the NLO corrections. The renormalization scales are set as two energy scales involved in the processes, i.e., $2m_Q$ and m_Z. Tables I and II show that the NLO corrections contribute significantly to the decay widths in both cases. The NLO corrections increase the decay width of $Z\to\eta_c+c+\bar{c}+X$ by ~34% for $\mu_R=2m_c$ and ~112% for $\mu_R=m_Z$; and they increase the decay width of $Z\to\eta_b+b+\bar{b}+X$ by ~28% for $\mu_R=2m_b$ and ~83% for $\mu_R=m_Z$.

In Figs. 4 and 5, the dependence of the decay widths on the renormalization scale is shown. After including the NLO corrections, the dependence of the decay widths on the renormalization scale is weakened. For $Z\to\eta_c+c+\bar{c}+X(Z\to\eta_b+b+\bar{b}+X)$, the decay width decreases by 77%(57%) at LO, and by 63%(39%) at NLO when μ_R varies from $2m_Q$ to m_Z. However, this dependence is still strong even including the NLO corrections.

Now, let us estimate the theoretical uncertainties for these decay widths. The main uncertainty sources include the renormalization scale, the heavy quark masses, and the radial wave functions at the origin.[4] For the uncertainties caused by the renormalization scale, we estimate them by

[4]The Monte Carlo numerical integration in the calculation would lead to an error. However, the error of the numerical integration is on the order of 10^{-2} keV for the η_c case, and 10^{-3} keV for the η_b case in our calculation. Thus, the error from the numerical integration is negligible.

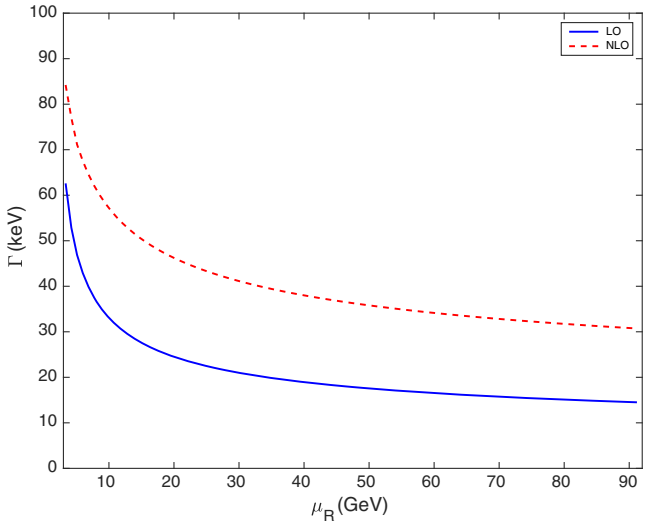

FIG. 4. The LO and NLO decay widths for $Z\to\eta_c+c+\bar{c}+X$ as functions of the renormalization scale μ_R.

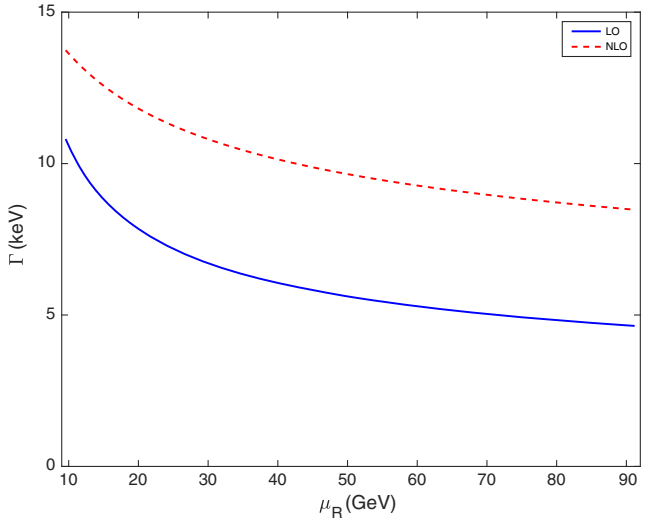

FIG. 5. The LO and NLO decay widths for $Z\to\eta_b+b+\bar{b}+X$ as functions of the renormalization scale μ_R.

varying the renormalization scale between two physical energy scales involved in the processes, i.e., $2m_Q$ and m_Z. Furthermore, we take the average values of the decay widths under the two choices of the renormalization scale as their central values. For the uncertainties caused by the heavy quark masses, we estimate them by varying the heavy quark masses in the ranges given in Eq. (20), i.e., $m_c=1.67\pm0.07$ GeV and $m_b=4.78\pm0.06$ GeV. For the radial wave functions at the origin, the authors of Ref. [61] did not give an error estimate. Since the potential used in Ref. [61] does not include the spin effect, the wave functions calculated in this way are accurate up to corrections of relative order v_Q^2. Therefore, we estimate the uncertainties by attaching an error of 30% of the central

value for η_c, and 10% of the central value for η_b. More explicitly, we take $|R_{\eta_c}(0)|^2 = 0.810 \pm 0.243$ GeV^3 and $|R_{\eta_b}(0)|^2 = 6.477 \pm 0.648$ GeV^3. Then we obtain

$$\Gamma^{\rm LO}_{Z\to\eta_c+c\bar{c}X} = 38.6^{+24.1+6.7+11.6}_{-24.1-5.5-11.6}\ \text{keV},$$
$$\Gamma^{\rm NLO}_{Z\to\eta_c+c\bar{c}X} = 57.6^{+26.7+10.3+17.3}_{-26.8-8.4-17.3}\ \text{keV}, \quad (23)$$

and

$$\Gamma^{\rm LO}_{Z\to\eta_b+b\bar{b}X} = 7.74^{+3.09+0.35+0.78}_{-3.09-0.40+0.78}\ \text{keV},$$
$$\Gamma^{\rm NLO}_{Z\to\eta_b+b\bar{b}X} = 11.1^{+2.7+0.5+1.2}_{-2.7-0.5-1.2}\ \text{keV}. \quad (24)$$

Here, the first error is caused by the renormalization scale, the second error is caused by the heavy quark mass, and the last error is caused by the radial wave function at the origin. From Eqs. (23) and (24), we can see that the largest error arises from the renormalization scale uncertainty for both η_c and η_b cases. Furthermore, we find that although the K factors are sensitive to the renormalization scale, they are insensitive to the heavy quark mass, e.g., when we vary the charm (bottom) quark mass from 1.60 GeV (4.72 GeV) to 1.74 GeV (4.84 GeV), the K factor changes from 1.50 (1.43) to 1.49 (1.44) for the η_c (η_b) case.

Adding the uncertainties in quadrature, we obtain

$$\Gamma^{\rm LO}_{Z\to\eta_c+c\bar{c}X} = 38.6^{+27.6}_{-27.3}\ \text{keV},$$
$$\Gamma^{\rm NLO}_{Z\to\eta_c+c\bar{c}X} = 57.6^{+33.4}_{-33.0}\ \text{keV}, \quad (25)$$

and

$$\Gamma^{\rm LO}_{Z\to\eta_b+b\bar{b}X} = 7.74^{+3.21}_{-3.21}\ \text{keV},$$
$$\Gamma^{\rm NLO}_{Z\to\eta_b+b\bar{b}X} = 11.1^{+3.0}_{-3.0}\ \text{keV}. \quad (26)$$

B. Differential decay widths

The differential distributions contain more information than the integrated decay widths, which can be used to test the current theory. Therefore, it is interesting to see the differential distributions of the two Z boson decay processes.

The energy fraction carrying by η_c or η_b in the processes can be defined as $z \equiv 2p_0 \cdot p_1/m_Z^2$. The LO and NLO differential decay widths $d\Gamma/dz$ for the processes $Z \to \eta_c + c + \bar{c} + X$ and $Z \to \eta_b + b + \bar{b} + X$ are shown in Figs. 6 and 7, respectively. Figures 6 and 7 confirm the importance of the NLO corrections. For the η_c production, the magnitude of $d\Gamma/dz$ is increased obviously at small and moderate z values and decreased slightly at higher z values. And for the η_b production, the magnitude of $d\Gamma/dz$ is increased at all z values. The uncertainties for $d\Gamma/dz$ are also shown in the figures, which are obtained by combining the uncertainties of the renormalization scale, the heavy quark mass, and the wave function at the origin.

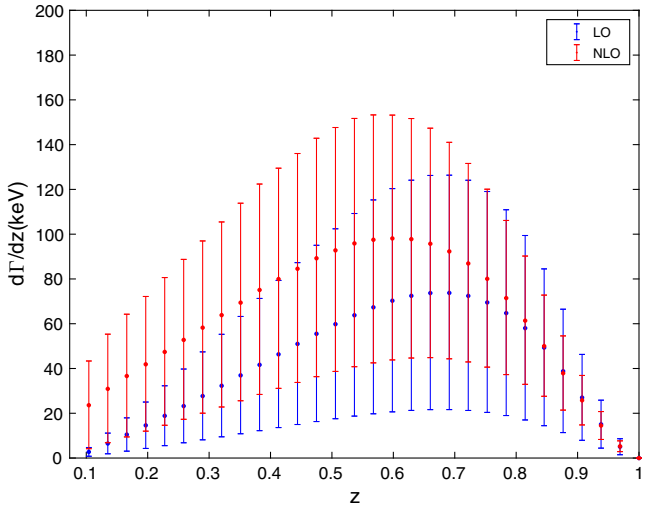

FIG. 6. The LO and NLO differential decay widths $d\Gamma/dz$ for $Z \to \eta_c + c + \bar{c} + X$. The error bars show the total uncertainties caused by the renormalization scale, the heavy quark mass, and the wave function at the origin, and the total uncertainties are obtained by adding each uncertainty in quadrature.

The momenta of heavy quarks in the final state can be determined experimentally using the heavy-flavor tagging technology. Therefore, the differential decay widths $d\Gamma/dm_{12}$ and $d\Gamma/dm_{23}$ can be measured experimentally, where $m_{12} \equiv \sqrt{(p_1+p_2)^2}$ and $m_{23} \equiv \sqrt{(p_2+p_3)^2}$ are invariant masses of two final-state particles. We present the LO and NLO differential decay widths $d\Gamma/dm_{12}$ and $d\Gamma/dm_{23}$ for $Z \to \eta_c + c + \bar{c} + X$ and $Z \to \eta_b + b + \bar{b} + X$ in Figs. 8, 9, 10, and 11, respectively. The uncertainties for these differential decay widths are also shown in these

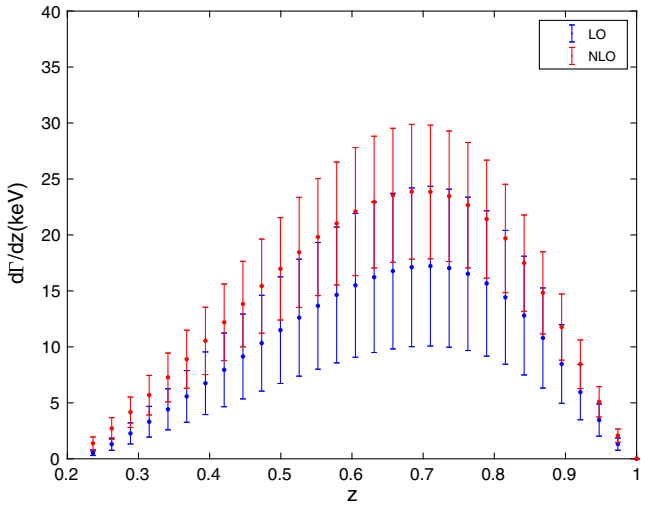

FIG. 7. The LO and NLO differential decay widths $d\Gamma/dz$ for $Z \to \eta_b + b + \bar{b} + X$. The error bars show the total uncertainties caused by the renormalization scale, the heavy quark mass, and the wave function at the origin, and the total uncertainties are obtained by adding each uncertainty in quadrature.

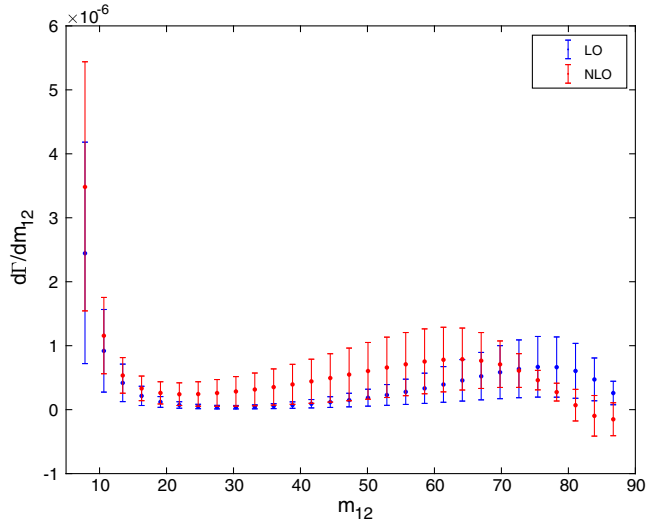

FIG. 8. The LO and NLO differential decay widths $d\Gamma/dm_{12}$ for $Z \to \eta_c + c + \bar{c} + X$. The error bars show the total uncertainties caused by the renormalization scale, the heavy quark mass, and the wave function at the origin, and the total uncertainties are obtained by adding each uncertainty in quadrature.

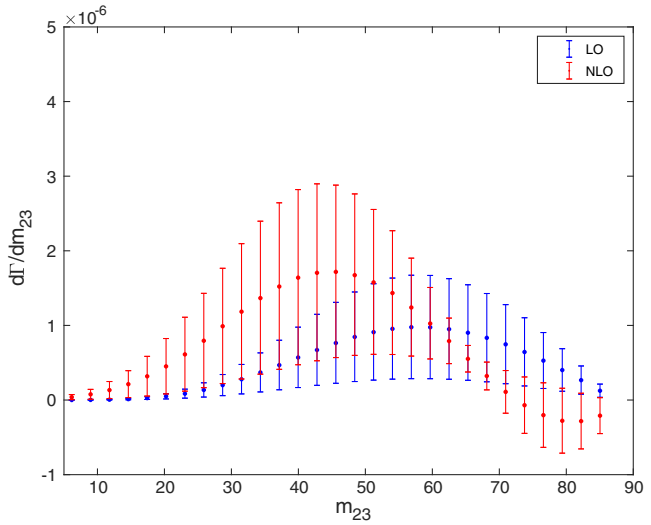

FIG. 10. The LO and NLO differential decay widths $d\Gamma/dm_{23}$ for $Z \to \eta_c + c + \bar{c} + X$. The error bars show the total uncertainties caused by the renormalization scale, the heavy quark mass, and the wave function at the origin, and the total uncertainties are obtained by adding each uncertainty in quadrature.

figures. From the figures, we can see that the differential decay widths $d\Gamma/dm_{12}$ and $d\Gamma/dm_{23}$ are changed significantly after including the NLO corrections, especially for the decay $Z \to \eta_c + c + \bar{c} + X$. Moreover, it is found that the NLO differential decay widths $d\Gamma/dm_{12}$ and $d\Gamma/dm_{23}$ are negative at the large m_{12} or m_{23} for $Z \to \eta_c + c + \bar{c} + X$. This indicates that the NLO corrections are negative and larger than the LO contribution in these phase space regions. In the boundary regions of the phase space, some large logarithmic terms often appear in the coefficients of the perturbation expansion, which may spoil the convergence of the perturbation series. In these boundary regions, it is necessary to resum these large logarithmic terms so as to obtain precise theoretical results. Because of these large logarithmic terms, if we calculate to a certain order (e.g., NLO) in these regions, we may obtain nonphysical negative results. Fortunately, in the considered processes, the absolute values of the negative contributions

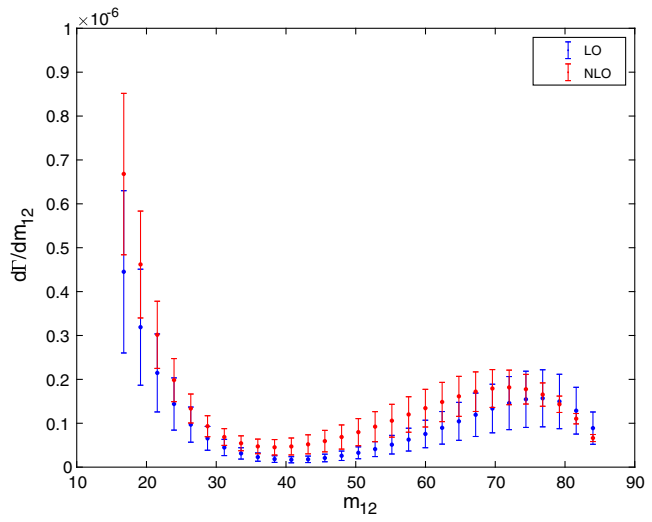

FIG. 9. The LO and NLO differential decay widths $d\Gamma/dm_{12}$ for $Z \to \eta_b + b + \bar{b} + X$. The error bars show the total uncertainties caused by the renormalization scale, the heavy quark mass, and the wave function at the origin, and the total uncertainties are obtained by adding each uncertainty in quadrature.

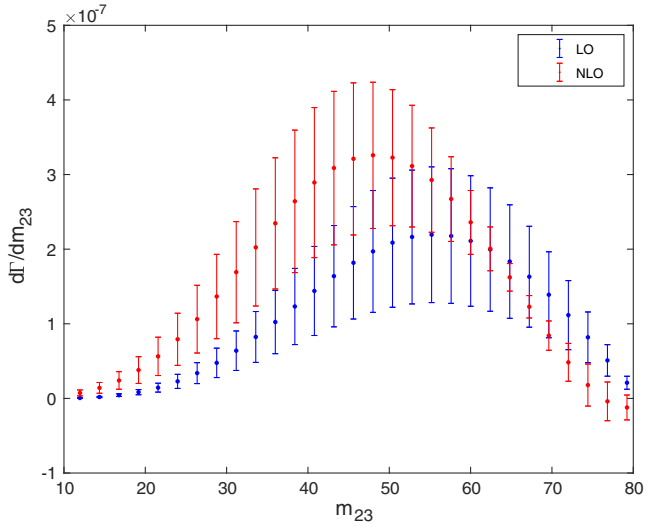

FIG. 11. The LO and NLO differential decay widths $d\Gamma/dm_{23}$ for $Z \to \eta_b + b + \bar{b} + X$. The error bars show the total uncertainties caused by the renormalization scale, the heavy quark mass, and the wave function at the origin, and the total uncertainties are obtained by adding each uncertainty in quadrature.

of these regions are not large. Thus, we believe that the differential decay widths for most regions of the phase space and the integrated decay widths, which are obtained in this paper, are reliable.

V. SUMMARY

In the present paper, we have studied the decays $Z \to \eta_c + c + \bar{c} + X$ and $Z \to \eta_b + b + \bar{b} + X$ up to NLO QCD accuracy. Integrated and differential decay widths of both decay processes are obtained, and the uncertainties for them are estimated. We find that the NLO corrections to the decay widths for $Z \to \eta_c + c + \bar{c} + X$ and $Z \to \eta_b + b + \bar{b} + X$ are significant. The dependence of the decay widths on the renormalization scale is very strong although the dependence is weakened after including the NLO corrections. This brings a big uncertainty to the theoretical predictions under the conventional renormalization scale setting. The higher-order corrections can reduce the uncertainty caused by the renormalization scale. However, it is very difficult to calculate the higher-order corrections beyond the NLO for these processes at present. In the literature, the principle of maximum conformality (PMC) scale-setting approach [63–66] has been suggested to eliminate such scale uncertainty, whose key idea is to determine the correct momentum flow of the process by using the nonconformal β-terms that govern the α_s running behavior with the help of renormalization group equation. As a comparison, we also calculate the integrated decay widths under the PMC scale setting. Following the standard PMC procedures to the decay width of $Z \to \eta_Q + Q + \bar{Q} + X$, we obtain $\Gamma^{\rm PMC}_{Z\to\eta_c+c\bar{c}X} = 95.4^{+34.1}_{-32.2}$ keV and $\Gamma^{\rm PMC}_{Z\to\eta_b+b\bar{b}X} = 14.7^{+1.7}_{-1.7}$ keV. Here, the PMC predictions of the decay width are independent to the choices of μ_R, and the errors come from the uncertainties of the heavy quark masses and the wave functions at the origin.

The cross sections for $e^+e^- \to Z \to \eta_Q + Q + \bar{Q} + X$ at the Z pole[5] can be derived from the decay widths $\Gamma_{Z\to\eta_Q+Q\bar{Q}X}$ through the formulas derived in the Appendix A1 of Ref. [67], i.e.,

$$\sigma_{e^+e^-\to\eta_Q+Q\bar{Q}X} = \frac{e^2(1-4\sin^2\theta_W+8\sin^4\theta_W)}{8\sin^2\theta_W\cos^2\theta_W m_Z\Gamma_Z^2} \times \Gamma_{Z\to\eta_Q+Q\bar{Q}X}. \quad (27)$$

Then we obtain

$$\sigma_{e^+e^-\to\eta_c+c\bar{c}X} = 1.37^{+0.80}_{-0.78}\ \text{pb}, \quad (28)$$

$$\sigma_{e^+e^-\to\eta_b+b\bar{b}X} = 0.264^{+0.072}_{-0.071}\ \text{pb}. \quad (29)$$

If the luminosity of a Z factory can be up to 10^{35} cm^{-2} s^{-1} [43], there are about 1.4×10^6 $\eta_c + c\bar{c}X$ events and 2.6×10^5 $\eta_b + b\bar{b}X$ events to be produced per operation year. Moreover, the background of the Z factory is clean. Therefore, the two production processes may be studied at a high luminosity Z factory.

ACKNOWLEDGMENTS

This work was supported in part by the Natural Science Foundation of China under Grants No. 12005028, No. 12175025, No. 12147116, and No. 12147102, by the China Postdoctoral Science Foundation under Grant No. 2021M693743, by the Fundamental Research Funds for the Central Universities under Grant No. 2020CQJQY-Z003, and by the Chongqing Graduate Research and Innovation Foundation under Grant No. ydstd1912.

[5]The γ-exchange contribution is negligibly small at the Z pole, which can be safely neglected.

[1] H. Fritzsch, Producing heavy quark flavors in hadronic collisions: A test of quantum chromodynamics, Phys. Lett. **67B**, 217 (1977).
[2] F. Halzen, CVC for gluons and hadroproduction of quark flavors, Phys. Lett. **69B**, 105 (1977).
[3] C. H. Chang, Hadronic production of J/ψ associated with a gluon, Nucl. Phys. **B172**, 425 (1980).
[4] E. L. Berger and D. L. Jones, Inelastic photoproduction of J/ψ and Υ by gluons, Phys. Rev. D **23**, 1521 (1981).
[5] T. Matsui and H. Satz, J/ψ suppression by quark-gluon plasma formation, Phys. Lett. B **178**, 416 (1986).
[6] G. T. Bodwin, E. Braaten, and G. P. Lepage, Rigorous QCD analysis of inclusive annihilation and production of heavy quarkonium, Phys. Rev. D **51**, 1125 (1995); **55**, 5853(E) (1997).
[7] N. Brambilla *et al.*, Heavy quarkonium: Progress, puzzles, and opportunities, Eur. Phys. J. C **71**, 1534 (2011) and references therein.
[8] A. Andronic, F. Arleo, R. Arnaldi, A. Beraudo, E. Bruna, D. Caffarri, Z. C. del Valle, J. G. Contreras, T. Dahms, A. Dainese *et al.*, Heavy-flavour and quarkonium production in the LHC era: From proton-proton to heavy-ion collisions, Eur. Phys. J. C **76**, 107 (2016).
[9] J. P. Lansberg, New observables in inclusive production of quarkonia, Phys. Rep. **889**, 1 (2020).
[10] A. P. Chen, Y. Q. Ma, and H. Zhang, A short theoretical review of charmonium production, Adv. High Energy Phys. **2022**, 7475923 (2022).
[11] R. Aaij *et al.* (LHCb Collabration), Measurement of the $\eta_c(1S)$ production cross-section in proton-proton

collisions via the decay $\eta_c(1S) \to p\bar{p}$, Eur. Phys. J. C **75**, 311 (2015).
[12] M. Butenschoen, Z. G. He, and B. A. Kniehl, η_c Production at the LHC Challenges Nonrelativistic-QCD Factorization, Phys. Rev. Lett. **114**, 092004 (2015).
[13] H. Han, Y. Q. Ma, C. Meng, H. S. Shao, and K. T. Chao, η_c Production at LHC and Indications on the Understanding of J/ψ Production, Phys. Rev. Lett. **114**, 092005 (2015).
[14] H. F. Zhang, Z. Sun, W. L. Sang, and R. Li, Impact of η_c Hadroproduction Data on Charmonium Production and Polarization Within NRQCD Framework, Phys. Rev. Lett. **114**, 092006 (2015).
[15] P. Pakhlov *et al.* (Belle Collaboration), Measurement of the $e^+e^- \to J/\psi c\bar{c}$ cross section at $\sqrt{s} \approx 10.6$ GeV, Phys. Rev. D **79**, 071101 (2009).
[16] Y. J. Li, G. Z. Xu, P. P. Zhang, Y. J. Zhang, and K. Y. Liu, Study of color octet matrix elements through J/ψ production in e^+e^- annihilation, Eur. Phys. J. C **77**, 597 (2017).
[17] B. Guberina, J. H. Kuhn, R. D. Peccei, and R. Ruckl, Rare decays of the Z^0, Nucl. Phys. **B174**, 317 (1980).
[18] W. Y. Keung, Off resonance production of heavy vector quarkonium states in e^+e^- annihilation, Phys. Rev. D **23**, 2072 (1981).
[19] K. J. Abraham, Bottonium production at LEP, Z. Phys. C **44**, 467 (1989).
[20] V. D. Barger, K. m. Cheung, and W. Y. Keung, Z-boson decays to heavy quarkonium, Phys. Rev. D **41**, 1541 (1990).
[21] K. Hagiwara, A. D. Martin, and W. J. Stirling, J/ψ production from gluon jets at LEP, Phys. Lett. B **267**, 527 (1991).
[22] E. Braaten, K. m. Cheung, and T. C. Yuan, Z^0 decay into charmonium via charm quark fragmentation, Phys. Rev. D **48**, 4230 (1993).
[23] S. Fleming, Electromagnetic production of quarkonium in Z^0 decay, Phys. Rev. D **48**, R1914 (1993).
[24] K. m. Cheung, W. Y. Keung, and T. C. Yuan, Color Octet Quarkonium Production at the Z Pole, Phys. Rev. Lett. **76**, 877 (1996).
[25] P. L. Cho, Prompt psi and Upsilon production at LEP, Phys. Lett. B **368**, 171 (1996).
[26] P. Ernstrom, L. Lonnblad, and M. Vanttinen, Evolution effects in Z^0 fragmentation into charmonium, Z. Phys. C **76**, 515 (1997).
[27] G. A. Schuler, Quarkonium production: Velocity scaling rules and long distance matrix elements, Int. J. Mod. Phys. A **12**, 3951 (1997).
[28] R. Li and J. X. Wang, Next-to-leading-order QCD correction to inclusive $J/\Psi(\Upsilon)$ production in Z^0 decay, Phys. Rev. D **82**, 054006 (2010).
[29] Q. L. Liao, Y. Yu, Y. Deng, G. Y. Xie, and G. C. Wang, Excited heavy quarkonium production via Z^0 decays at a high luminosity collider, Phys. Rev. D **91**, 114030 (2015).
[30] T. C. Huang and F. Petriello, Rare exclusive decays of the Z boson revisited, Phys. Rev. D **92**, 014007 (2015).
[31] A. K. Likhoded and A. V. Luchinsky, Double charmonia production in exclusive Z boson decays, Mod. Phys. Lett. A **33**, 1850078 (2018).
[32] G. T. Bodwin, H. S. Chung, J. H. Ee, and J. Lee, Z-boson decays to a vector quarkonium plus a photon, Phys. Rev. D **97**, 016009 (2018).
[33] Z. Sun and H. F. Zhang, Next-to-leading-order QCD corrections to the decay of Z boson into $\chi_c(\chi_b)$, Phys. Rev. D **99**, 094009 (2019).
[34] H. S. Chung, J. H. Ee, D. Kang, U. R. Kim, J. Lee, and X. P. Wang, Pseudoscalar quarkonium + gamma production at NLL + NLO accuracy, J. High Energy Phys. 10 (2019) 162.
[35] X. C. Zheng, C. H. Chang, and X. G. Wu, NLO fragmentation functions of heavy quarks into heavy quarkonia, Phys. Rev. D **100**, 014005 (2019).
[36] Z. Sun, The studies on $Z \to \Upsilon(1S) + g + g$ at the next-to-leading-order QCD accuracy, Eur. Phys. J. C **80**, 311 (2020).
[37] Z. Sun and H. F. Zhang, Comprehensive studies of Υ inclusive production in Z boson decay, J. High Energy Phys. 06 (2021) 152.
[38] X. C. Zheng, C. H. Chang, X. G. Wu, X. D. Huang, and G. Y. Wang, Inclusive production of heavy quarkonium ηQ via Z boson decays within the framework of nonrelativistic QCD, Phys. Rev. D **104**, 054044 (2021).
[39] Z. Sun, X. Luo, and Y. Z. Jiang, Impact of $Z \to \eta_{c,b} + g + g$ on the inclusive $\eta_{c,b}$ meson yield in Z-boson decay, Phys. Rev. D **106**, 034001 (2022).
[40] H. Baer, T. Barklow, K. Fujii, Y. Gao, A. Hoang, S. Kanemura, J. List, H. E. Logan, A. Nomerotski, M. Perelstein *et al.*, The international linear collider technical design report—Volume 2: Physics, arXiv:1306.6352.
[41] A. Abada *et al.* (FCC Collaboration), FCC physics opportunities: Future circular collider conceptual design report Volume 1, Eur. Phys. J. C **79**, 474 (2019).
[42] J. B. Guimarães da Costa *et al.* (CEPC Study Group Collaboration), CEPC conceptual design report: Volume 2—physics & detector, arXiv:1811.10545.
[43] J. P. Ma and Z. X. Zhang (The Super Z-Factory Group Collaboration), Preface, Sci. China: Phys., Mech. Astron. **53**, 1947 (2010).
[44] J. Erler, S. Heinemeyer, W. Hollik, G. Weiglein, and P. M. Zerwas, Physics impact of GigaZ, Phys. Lett. B **486**, 125 (2000).
[45] W. Buchmuller and S. H. H. Tye, Quarkonia and quantum chromodynamics, Phys. Rev. D **24**, 132 (1981).
[46] X. C. Zheng, Z. Y. Zhang, and X. G. Wu, Fragmentation functions for a quark into a spin-singlet quarkonium: Different flavor case, Phys. Rev. D **103**, 074004 (2021).
[47] J. G. Korner, D. Kreimer, and K. Schilcher, A practicable γ_5-scheme in dimensional regularization, Z. Phys. C **54**, 503 (1992).
[48] M. Beneke and V. A. Smirnov, Asymptotic expansion of Feynman integrals near threshold, Nucl. Phys. **B522**, 321 (1998).
[49] M. Klasen, B. A. Kniehl, L. N. Mihaila, and M. Steinhauser, J/ψ plus jet associated production in two-photon collisions at next-to-leading order, Nucl. Phys. **B713**, 487 (2005).
[50] T. Hahn, Generating Feynman diagrams and amplitudes with FeynArts 3, Comput. Phys. Commun. **140**, 418 (2001).
[51] R. Mertig, M. Bohm, and A. Denner, Feyn Calc: Computer-algebraic calculation of Feynman amplitudes, Comput. Phys. Commun. **64**, 345 (1991).
[52] V. Shtabovenko, R. Mertig, and F. Orellana, New developments in FeynCalc 9.0, Comput. Phys. Commun. **207**, 432 (2016).

[53] F. Feng, $Apart: A generalized mathematica apart function, Comput. Phys. Commun. **183**, 2158 (2012).
[54] A. V. Smirnov, Algorithm FIRE: Feynman Integral REduction, J. High Energy Phys. 10 (2008) 107.
[55] T. Hahn and M. Perez-Victoria, Automatized one loop calculations in four-dimensions and D-dimensions, Comput. Phys. Commun. **118**, 153 (1999).
[56] G. P. Lepage, A new algorithm for adaptive multidimensional integration, J. Comput. Phys. **27**, 192 (1978).
[57] B. W. Harris and J. F. Owens, The Two cutoff phase space slicing method, Phys. Rev. D **65**, 094032 (2002).
[58] A. Bassetto, M. Ciafaloni, and G. Marchesini, Jet structure and infrared sensitive quantities in perturbative QCD, Phys. Rep. **100**, 201 (1983).
[59] A. Denner, Techniques for calculation of electroweak radiative corrections at the one loop level and results for W physics at LEP-200, Fortschr. Phys. **41**, 307 (1993).
[60] W. Beenakker, S. Dittmaier, M. Kramer, B. Plumper, M. Spira, and P. M. Zerwas, NLO QCD corrections to $t\bar{t}$H production in hadron collisions, Nucl. Phys. **B653**, 151 (2003).
[61] E. J. Eichten and C. Quigg, Mesons with beauty and charm: Spectroscopy, Phys. Rev. D **49**, 5845 (1994).
[62] R. L. Workman (Particle Data Group), Review of particle physics, Prog. Theor. Exp. Phys. **2022**, 083C01 (2022).
[63] S. J. Brodsky and X.-G. Wu, Scale setting using the extended renormalization group and the principle of maximum conformality: The QCD coupling constant at four loops, Phys. Rev. D **85**, 034038 (2012).
[64] S. J. Brodsky and X.-G. Wu, Eliminating the Renormalization Scale Ambiguity for Top-Pair Production Using the Principle of Maximum Conformality, Phys. Rev. Lett. **109**, 042002 (2012).
[65] M. Mojaza, S. J. Brodsky, and X.-G. Wu, Systematic All-Orders Method to Eliminate Renormalization-Scale and Scheme Ambiguities in Perturbative QCD, Phys. Rev. Lett. **110**, 192001 (2013).
[66] S. J. Brodsky, M. Mojaza, and X.-G. Wu, Systematic scale-setting to all orders: The principle of maximum conformality and commensurate scale relations, Phys. Rev. D **89**, 014027 (2014).
[67] X. C. Zheng, C. H. Chang, T. F. Feng, and Z. Pan, NLO QCD corrections to $B_c(B_c^*)$ production around the Z pole at an e^+ e^- collider, Sci. China Phys. Mech. Astron. **61**, 031012 (2018).